Contents lists available at ScienceDirect
Aerospace Science and Technology
www.elsevier.com/locate/aescte

Investigation of boundary-layer ejecting for resistance to back pressure in an isolator

Yubao He, Hongyan Huang, Daren Yu *

School of Energy Science and Engineering, Harbin Institute of Technology, Harbin, 150001, PR China

ARTICLE INFO

Article history:
Received 22 October 2015
Received in revised form 27 March 2016
Accepted 18 April 2016
Available online xxxx

Keywords:
Shock/boundary layer interaction
Inlet unstart
Flow control
Ejecting
Cracking gas

ABSTRACT

In order to increase resistance to back pressure in an inlet isolator, an ejecting flow control method is applied in this paper. For the sake of checking out the control effect, test cases with air and cracking gas ejecting are completed in $M = 2.41$ inlet. According to the numerical results, the resistance to back pressure with air and cracking gas ejecting is increased by 15% and 11.76% at $P_{t,eje} = 1.07 \times 10^6$ Pa and $P_{t,eje} = 4 \times 10^6$ Pa, respectively, which indicates that the control method is effective. The flow field characteristic with air and cracking gas ejecting is compared to reveal the difference of shock/boundary layer interaction and the propagating path of adverse pressure gradient. As the back pressure increased, the adverse pressure gradient can propagate upstream along the wide range of aerodynamic subsonic bands far from the wall, which are formed by the large-scale Mach stem of Mach reflection. Furthermore, the influence of ejecting total pressure on flow field is further analyzed to understand the physical mechanism of the resistance to back pressure. The increase of the ejecting total pressure can indirectly increase the ejecting momentum and decrease the ejecting dynamic viscosity, which prompts the random motion of molecules in the shear layer between ejecting flow and core flow, thereby increasing the mixing of the momentum, mass and energy to narrow the subsonic band and suppress the adverse pressure gradient.

1. Introduction

The inlet and isolator are important aerodynamic components in an air-breathing engine [1,2]. In these compression systems, shock-wave/boundary-layer interaction (SWBLI) is a complex physical phenomenon of compressible viscous flow. After a type of pre-combustion shock train inside the inlet undergoes multiple reflections, it can thicken boundary layer [3], cause flow distortions [4] and even induce flow separation [5]. At this point, if the combustor back pressure is too high for the shock-train length to match, unstart can occur. It is therefore critical to effectively control the boundary-layer flow to improve the performance of propulsion system and increase the stability margins.

Methods to control or minimize shock-induced flow separation have been proposed and are mainly classified as passive and active control. Control nature, whether passive or active, manages to increase the momentum of fluid near the wall so that the boundary layer can withstand the adverse pressure gradient imposed by incident shock or heat release at high equivalence ratio. Of these methods, since the suction control was first brought forward, its application has lasted to the present time. It can remove the low energy boundary-layer flow and reduce the size of the separation through a perforated domain [6–8]. Although suction provides many benefits to the propulsion system, its use often comes at a cost of increased drag and weight of the aircraft, thereby increasing the system complexity [9]. Another attractive control technique is micro vortex generators such as the micro-ramps. Saad et al. [10] performed the wind tunnel experiments at Mach 5 with two micro-ramps of different sizes to investigate the control of shock-wave/boundary-layer interaction and revealed the mechanism of the flow control device through schlieren visualization technique, surface flow visualization, and a new type of luminescent measurement technique such as infrared thermography [11]. Oorebeek et al. [12] devised a normal shock experiment with a supersonic inflow of Mach 1.35 to investigate the vortex generator and bleed effectiveness suppressing flow separation. They found that the vortex generator is similar to the bleed and can considerably reduce the separation bubble size, thereby improving the diffuser performance. Martis et al. [13] conducted a three dimensional numerical investigation to analyze the effect of micro-ramps on the separated swept shock-wave/boundary layer interactions. They analyzed the parametric influence of the height, width, and spacing

* Corresponding author. Address for correspondence: No. 92, West Da-Zhi Street, Harbin, Heilongjiang, 150001, PR China.
E-mail address: yudaren@hit.edu.cn (D. Yu).

http://dx.doi.org/10.1016/j.ast.2016.04.016
1270-9638/

Please cite this article in press as: Y. He et al., Investigation of boundary-layer ejecting for resistance to back pressure in an isolator, Aerosp. Sci. Technol. (2016), http://dx.doi.org/10.1016/j.ast.2016.04.016

Nomenclature

H_{ne}	height of the Aft-Facing Step Nozzle entrance
h_{iso}	height of the isolator
I	turbulent intensity
Imp_{bp}	the increased backpressure ratio
k	turbulent kinetic energy
L_{total}	total length of inlet model
L_1	the horizontal length of the first ramp in Aft-Facing Step Nozzle
L_2	the horizontal length of the second ramp in Aft-Facing Step Nozzle
M	Mach number
m	mass flow rate
PR	ratio of backpressure to freestream static pressure
P	pressure
R_{e}	Reynolds number
T	temperature
WE	with ejecting
WOE	without ejecting
v	mass-weighted average velocity at the entrance of AFST
x	X-axis coordinate
y	Y-axis coordinate
α	angle of attack
μ	dynamic viscosity
δ_1	first ramp angle
δ_2	second ramp angle
δ_3	cowl angle
δ_4	divergence angle
ω	turbulent dissipation rate

Subscripts

b	backpressure
c	cowl wall
cap	capture of inlet model
eje	ejecting condition
iso	isolator
r	ramp wall
s	static condition
t	total condition
∞	freestream condition

of the micro-ramps and drew a conclusion that the micro-ramps can significantly delay the boundary-layer separation. Alternatively, the larger height of micro-ramps can be more conductive to delaying the flow separation. Although the vortex generator can induce pairs of counter-rotating streamwise vortices to mix the high momentum fluid of core flow with the near-wall low momentum boundary layer flow, there is still a potential hazard of engine damage if the structure is destroyed [14]. Recently, an array of continuous air jet vortex generators (AJVGs) on upstream surface of separation bubble is used to successfully reduce the separation bubble size through inducing the periodical change of velocity which can redistribute the boundary-layer momentum, but the effectiveness is reduced at off design conditions [15]. However, the most of research mainly focuses on a single point control of separation bubble. Fewer investigations on the back pressure control can be seen. It is thus necessary to utilize a control method in inlet model to restrain the upstream propagation of adverse pressure gradient and simultaneously avoid several disadvantages of above methods.

The motivation for this work presented in this paper is derived from the idea that the turbopump system inside the supersonic or hypersonic aircraft has the ability to compress the cracking gas in the cooling channel of scramjet, a portion of high temperature cracking gas is expected to eject into the isolator to increase resistance to back pressure. Therefore, in this paper, test cases with air and cracking gas ejecting are conducted in $M = 2.41$ inlet to check out the control effect and initially grasp the flow field characteristic. The flow field characteristic with air and cracking gas ejecting is compared to reveal the difference of shock/boundary layer interaction and the propagating path of adverse pressure gradient. Furthermore, on that basis, the influence of ejecting total pressure on flow field is further analyzed to understand the physical mechanism of the resistance to back pressure.

2. Numerical approach

In the current investigation, the flow simulations are performed by ANSYS® Fluent 14.5. It uses a finite-volume technique with second-order upwind discretization to solve the two-dimensional compressible Reynolds-averaged Navier–Stokes equations and species transport equations without reactions. Flux vector splitting is done using advection upstream splitting method for approximation of convective flux functions. Implicit residuals smoothing, a multiple-grid method and full multigrid (FMG) initialization are applied to accelerate convergence. Additionally, the separation prediction is very important in many compression systems both for internal and external flows. Currently, the most prominent two-equation models in aerodynamic area are the k–ω based models of Menter [16]. The k–ω based Shear-Stress-Transport (SST) model is designed to give highly accurate predictions of the onset and the amount of flow separation under adverse pressure gradients by the introducing the transport effects into the formulation of the eddy-viscosity. The superior performance of this model has been demonstrated in a considerable number of validation studies [17]. So, the turbulent velocity profile in the paper is modeled by a two-equation k–ω SST turbulence model.

Since the discretization error and rounding error greatly depend on the grid resolution, a sequence of multiblock structured grids is tested to determine the grid sensitivity and validate the numerical approach according to the aerodynamic experiment by Reinartz at the Aachen Jet Propulsion Laboratory [18]. The sketch of the similar inlet model is shown in Fig. 1. Fig. 2 gives computational domain discretized by using a structured grid with regularly shaped cells and corresponding set of boundary conditions. Since the horizontal incoming freestream has already been compressed by the first ramp which has been completely neglected according to Ref. [18], the flow condition in Table 1 is applied to the far field at the left boundary of the domain while the pressure outlet is set by using a characteristic boundary condition, i.e. defining the static pressure equal to the incoming static pressure. The no-slip condition, adiabatic walls and zero normal-pressure gradients are imposed on all solid walls.

As reported in Ref. [18], the three dimensional effect of isolator almost had no effect on the pressure distribution on a symmetric surface in the numerical algorithm validation process. Therefore, a two-dimensional model is used for the numerical validation, and the impact of a small amount of flow separation on the side wall on the formation of shock wave is then ignored for the symmetric surface. The coarse grid, fine grid, and dense grid which clusters near the solid wall contains 610×65, 1117×130, and 2234×260 cells in the x and y directions, respectively. For the fine grid and

Please cite this article in press as: Y. He et al., Investigation of boundary-layer ejecting for resistance to back pressure in an isolator, Aerosp. Sci. Technol. (2016), http://dx.doi.org/10.1016/j.ast.2016.04.016

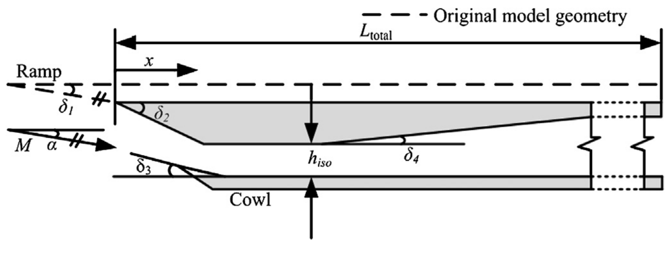

Fig. 1. Sketch of similar inlet model in [18].

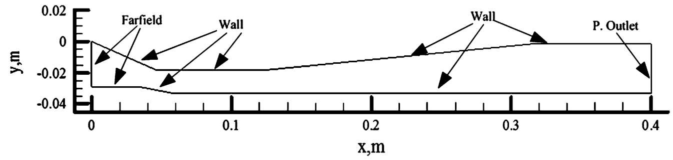

Fig. 2. Corresponding computational domain and boundary conditions.

Table 1
Flow condition and calculated turbulence parameters.

M (–)	P_t (Pa)	T_t (K)	R_e (m^{-1})	α (deg)	I (%)	k (m^2/s^2)	ω (s^{-1})
2.41	5.40×10^5	305	5.07×10^7	-10	2.78	3.82×10^2	9.80×10^3

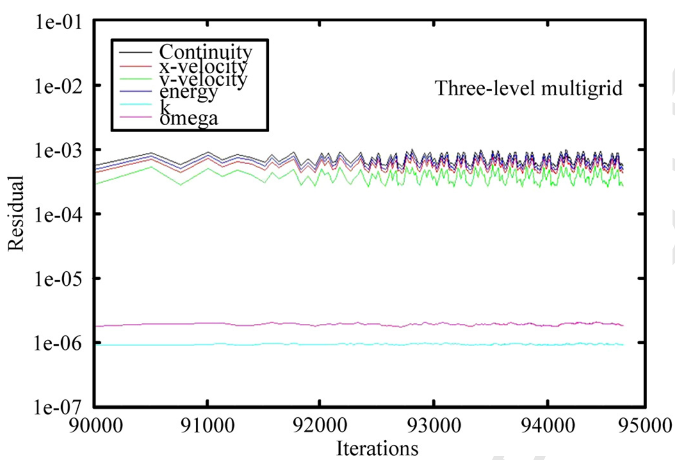

Fig. 3. Residual for supersonic inlet computation.

dense grid, the grids are refined in flow domain, except for the boundary-layer region. This maximum value of $y+$ is kept near 30 for all walls, since the standard wall function is used. To capture the shock-wave/boundary-layer interactions correctly, the residuals of governing equation are monitored in Fig. 3. The numerical solution is considered converged after approximately 93000 iterations for the three-level multigrid. In the convergence process, the residual of continuity, momentum and energy equation reaches the minimum value after dropping three orders of magnitude. The residual of turbulence equation falls over five orders of magnitude and then keeps unchanged. For other convergence criterion adopted, the mass deviation between inlet and outlet is kept less than 0.5% and typical major variable gradients are kept almost unchanged by vertex-average monitoring. As shown in Fig. 4, the overall variation trend of surface pressure from three different grid-refinement levels agrees well with the experimental data. Slight difference can be seen between the three grids because of the complex dynamic behavior of shock-wave/boundary-layer interactions and flow separation. The comparison of numerical schlieren achieved from the fine grid with experimental one is also performed in Fig. 5. The fine grid correctly captures the shock wave

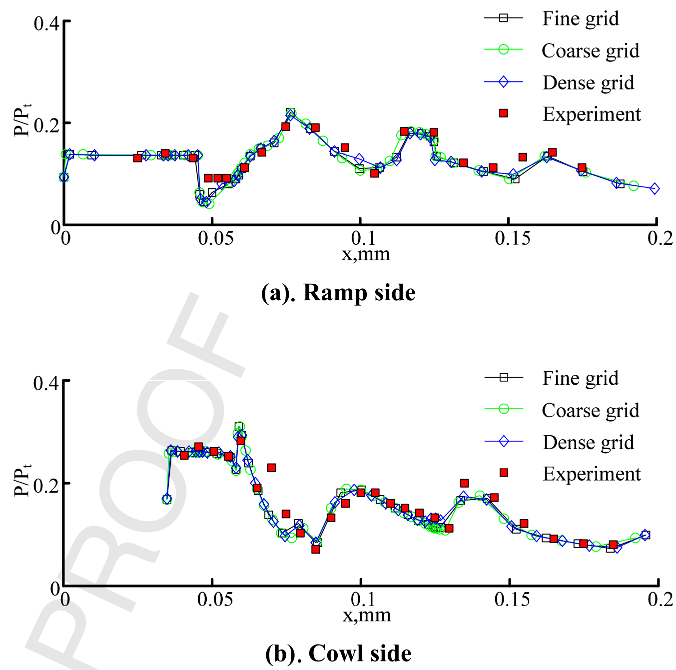

Fig. 4. Surface pressure distributions on Ramp and Cowl walls at $M = 2.41$, $PR = 0.0$.

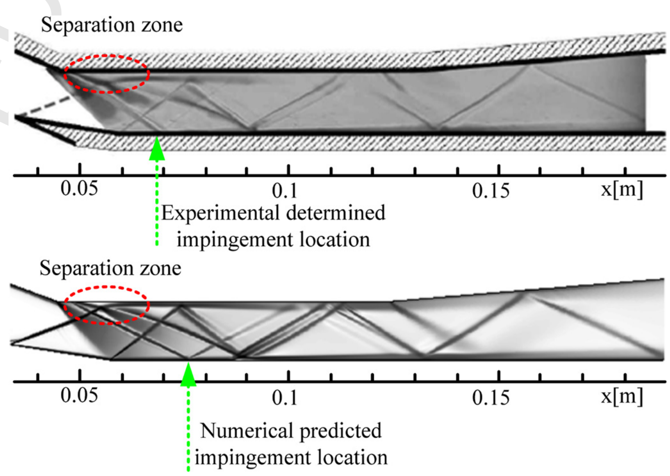

Fig. 5. Experimental and numerical schlieren pictures at $M = 2.41$, $PR = 0.0$.

pattern, the flow separation, and the approximate boundary-layer thickness, but it does not present the detail of shear layer and the shedding process of vortex. The computed flow separation appears to be smaller than what was observed in the experiment, and so the separation-induced shock is weaker and impinges downstream of location measured the experiment. The reason for the discrepancy is probably the non-uniform effect of incoming flow, three-dimensional effect, heat transfer effect, and the deficiency of the turbulence model. Thus, the fine grid will be selected for the subsequent study.

3. Description of inlet model with Aft-Facing Step Nozzle

To investigate and validate the impact of boundary-layer ejecting on the resistance to back pressure, an Aft-Facing Step Nozzle (AFSN), which can provide high recovery coefficient of total pressure as reported in Ref. [19], is integrated to the inlet model along the Ramp and Cowl walls in Fig. 1. Fig. 6 gives the sketch of the 2D simplified Aft-Facing Step Nozzle (AFSN) in [19], which is referred to as ejecting nozzle or nozzle in current paper. It mainly

Please cite this article in press as: Y. He et al., Investigation of boundary-layer ejecting for resistance to back pressure in an isolator, Aerosp. Sci. Technol. (2016), http://dx.doi.org/10.1016/j.ast.2016.04.016

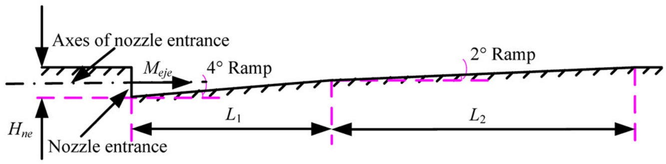

Fig. 6. Sketch of the 2D simplified Aft-Facing Step Nozzle (AFSN) in [19].

consists of the 4 deg ramp and 2 deg ramp with the length of $L_1 = 8.58$ mm and $L_2 = 11.45$ mm, respectively. The entrance height of the Aft-Facing Step Nozzle is $H_{\text{ne}} = 1$ mm. In the present paper, the process of flow control using high pressure gas from the Aft-Facing Step Nozzle to control downstream boundary-layer development is referred to as “boundary-layer ejecting” or “ejecting”. The entrance condition of the Aft-Facing Step Nozzle is referred to as “ejecting condition”. For example, the high total pressure at the Aft-Facing Step Nozzle entrance is referred to as ejecting total pressure. Fig. 7 shows the sketch of the 2D simplified inlet model with the two Aft-Facing Step Nozzles highlighted by the red circle. The inlet model is a two-dimensional mixed-compression system. Due to the size limitation of wind tunnel, the geometry only contains one external compression, where the angle of ramp is $\delta_2 = 21.5$ deg. And the flow deflection angles through the two-stage cowl shock wave are 12 deg and 9.5 deg, respectively. The height of isolator, denoted by h_{iso}, is 15 mm and the overall length of the inlet is $L_{\text{total}} = 400$ mm. In the simulation, the flow condition is applied according to Table 1, and the ejecting condition at the entrance of nozzle is specified as $P_{\text{t,eje}} = 1.07 \times 10^6$ Pa, $P_{\text{s,eje}} = 7.30 \times 10^4$ Pa, and $T_{\text{t,eje}} = 1111$ K. The ejecting gas chosen is air, and the gaseous methane of cracking gas for comparison, respectively. Patch initialization method is utilized to simulate a specific back pressure induced by combustor. When the reference

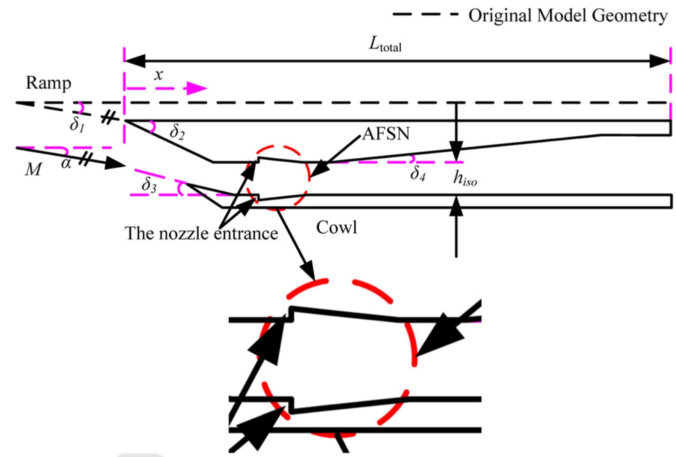

Fig. 7. Sketch of the 2D simplified inlet model with the two Aft-Facing Step Nozzles. (For interpretation of the references to color in this figure, the reader is referred to the web version of this article.)

inlet integrates with the AFSN, the distance of the starting point of the AFSN from separation bubble near the shoulder can be determined through the CFD multi-iteration to avoid unstart which is caused by the ejecting pressure.

4. Results and discussion

4.1. Influence of air ejecting on shock/boundary layer interaction

Fig. 8 shows the unthrottled flow structure without ejecting nozzle. When the supersonic flow is compressed by the cowl, two-stage cowl shocks are subsequently induced, which cause

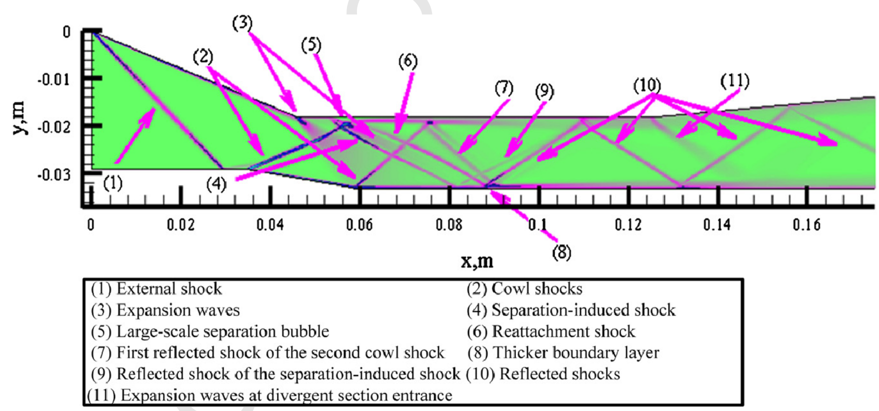

Fig. 8. Flow patterns of shock/boundary layer interaction without ejecting at the fore part of the duct, $M = 2.41$, $PR = 0.0$.

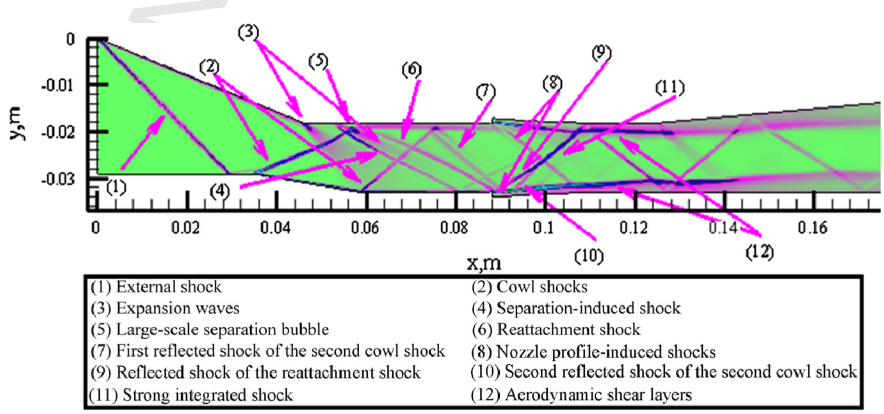

Fig. 9. Flow patterns of shock/boundary layer interaction with ejecting at the fore part of the duct, $M = 2.41$, $PR = 0.0$.

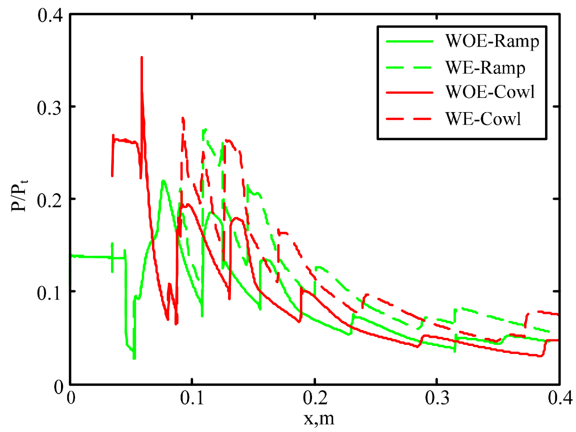

Fig. 10. Pressure distribution on the ramp and cowl with and without ejecting nozzle at $M = 2.41$, $PR = 0.0$.

the boundary layer to separate and form the large-scale separation bubble near the impingement point of the first-stage cowl shock, thereby generating complex background shock wave: 1) the separation-induced shock after impinging on the cowl wall thickens boundary layer; 2) the expansion waves are formed near the vertex of separation bubble; 3) the first-stage cowl shock tends to bend in the interaction region between expansion waves and cowl shock; 4) the reattachment shock and first reflected shock of the second cowl shock impinge on the closer region of cowl wall and significantly thicken the boundary layer, but do not induce the flow separation; 5) these shock waves interact with each other and undergo multiple reflections, which further form more complex flow structure.

Fig. 9 shows the unthrottled flow structure with ejecting nozzle. One can see that the flow structure upstream the ejecting nozzle is exactly the same to the flow without ejecting nozzle, which means that the integrated Aft-Facing Step Nozzle has no negative

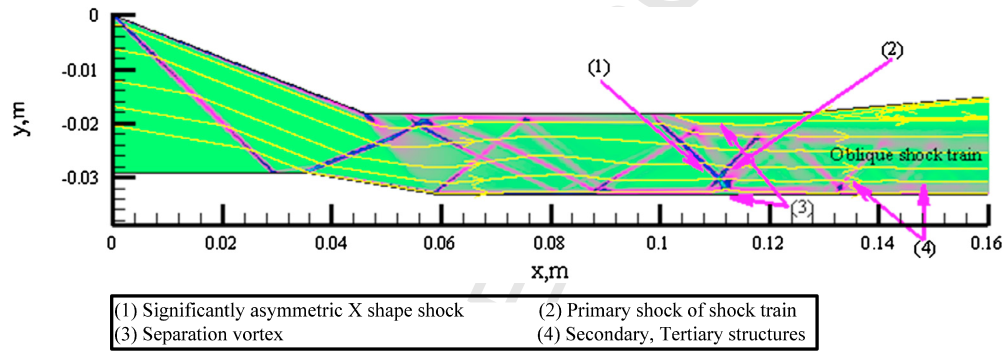

(a). $P_b/P_s = 7.0$

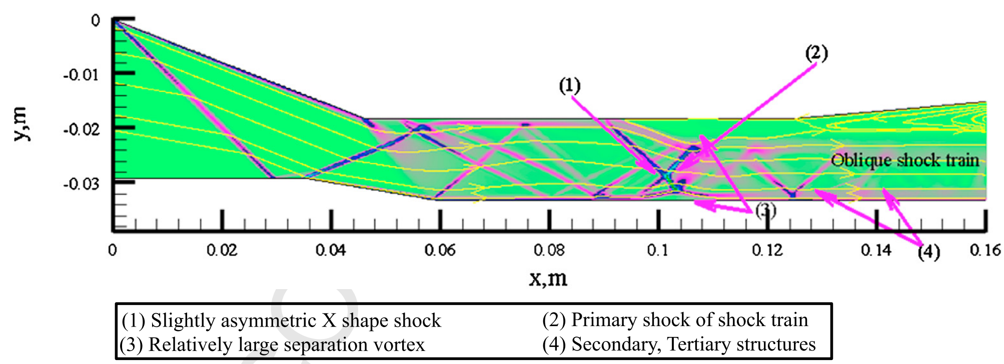

(b). $P_b/P_s = 8.0$

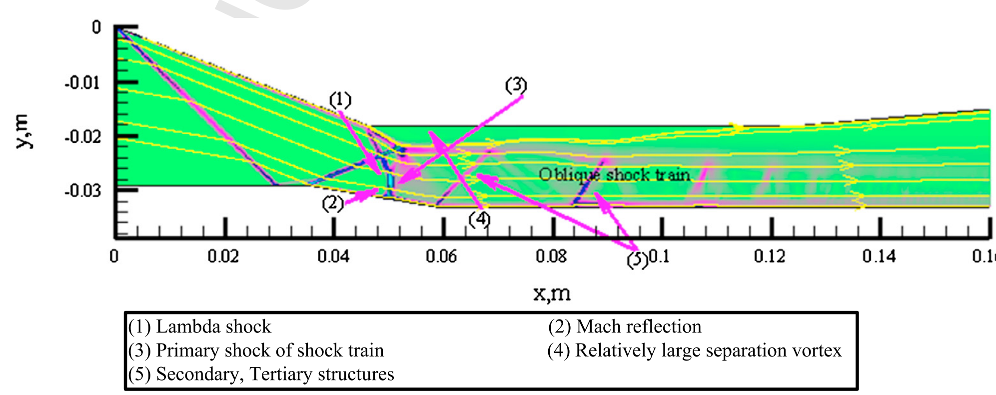

(c). $P_b/P_s = 8.5$

Fig. 11. Throttled flow patterns of shock/boundary layer interaction without ejecting at the fore part of the duct, $M = 2.41$.

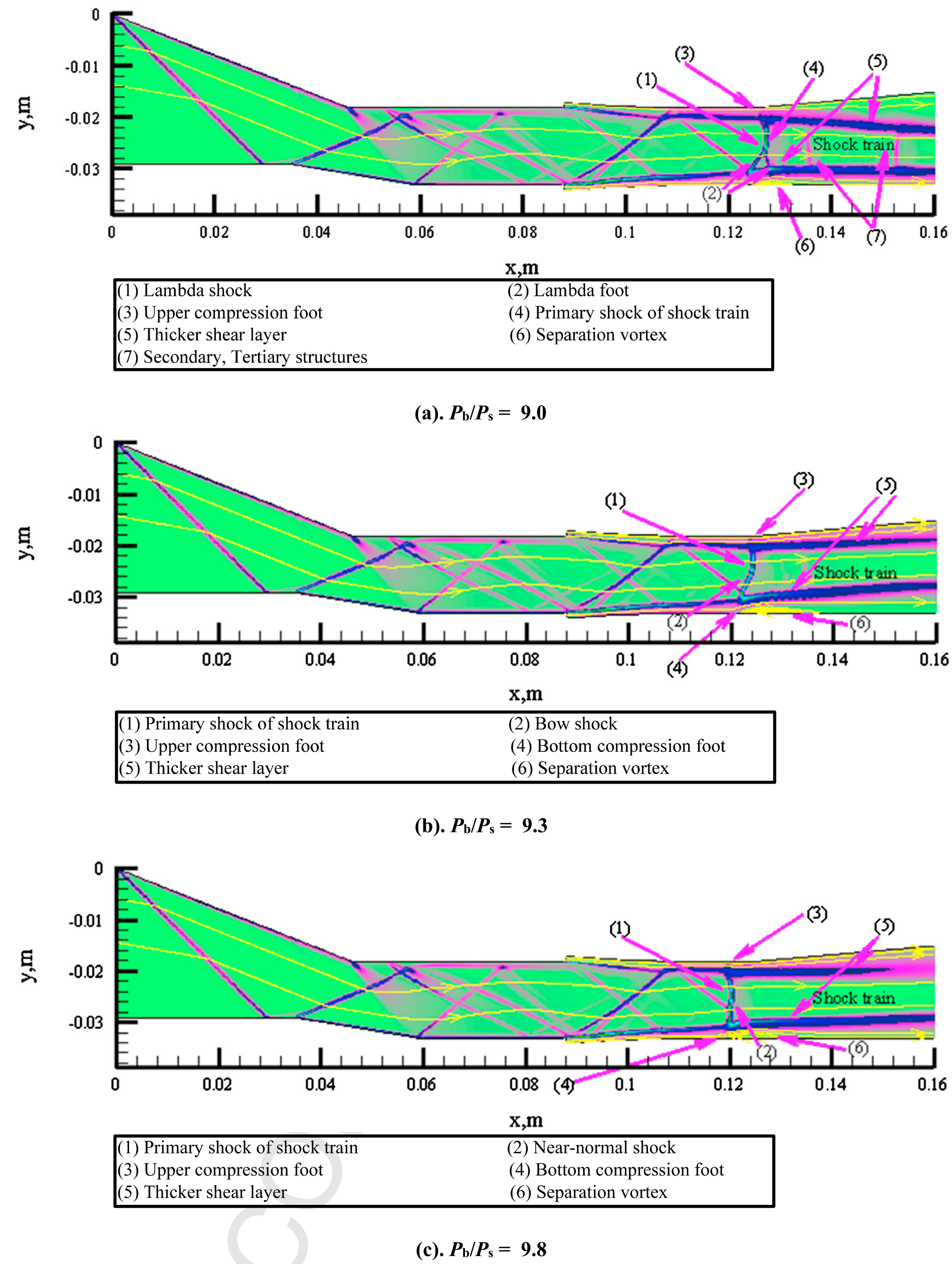

Fig. 12. Throttled flow patterns of shock/boundary layer interaction with ejecting at the fore part of the duct, $M = 2.41$.

effect on the separation bubble near the shoulder any more. In addition, the aerodynamic shear layer can be seen obviously from the schlieren picture mainly due to the fact that there is the relatively large velocity gradient between the near-wall ejecting flow and core flow. Meanwhile, a strong shock, which is integrated with reflected shock of the reattachment shock, second reflected shock of the second cowl shock and nozzle profile-induced weak shock, impinges on the ramp wall and sharply decelerates the ejecting flow, which leads to form the comparatively thick shear layer. However, the shear layer is apparently thinned by the acceleration of expansion waves at the entrance of divergent section. It is not until the reflected shocks are gradually weaken and the full mixing of the ejecting flow and core flow that the shear layer almost cannot be discerned at the rear part of the divergent section. The similar change of shear layer near the cowl wall can be obtained. Therefore, although the introduction of ejecting nozzle can induce more complex flow structure, its application does not cause the inlet unstart, which indicates that the position of nozzle in this paper can be accepted to subsequent study.

Fig. 10 gives the pressure distribution normalized by the incoming total pressure P_t. The pressure distribution on the ramp and cowl shows a similar wavelike shape compared to the flow without ejecting nozzle. It is evident that the pressure distribution before the ejecting nozzle is almost the same (the starting point of ejecting nozzle is at $x = 0.088$ m) while a series of shocks behind the ejecting nozzle result in an obvious pressure rising and corresponding wave peak and trough, whether on the ramp or the cowl, all locate ahead of the one without ejecting nozzle. Therefore, it can be concluded that the introduction of the ejecting nozzle can increase the shock strength and change the shock reflection point.

Please cite this article in press as: Y. He et al., Investigation of boundary-layer ejecting for resistance to back pressure in an isolator, Aerosp. Sci. Technol. (2016), http://dx.doi.org/10.1016/j.ast.2016.04.016

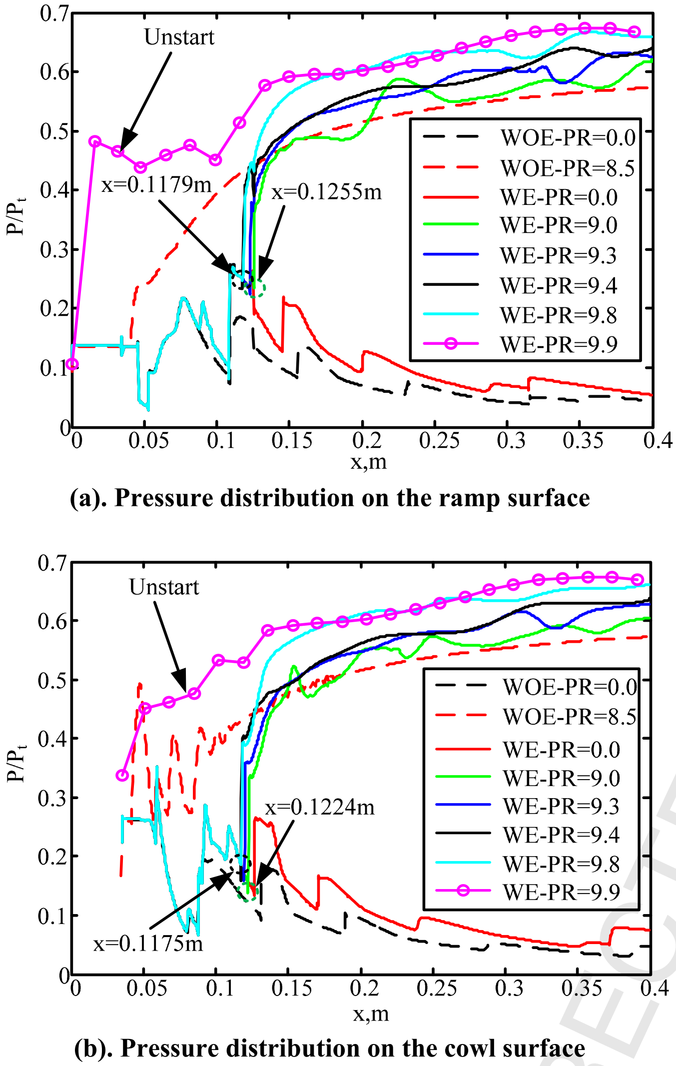

Fig. 13. Throttled pressure distributions of shock/boundary layer interaction with ejecting at $M = 2.41$.

4.2. Influence of air ejecting on shock/boundary layer interaction with throttling

Fig. 11 shows the throttled flow structure without ejecting nozzle. It can be seen that shock train originally locates downstream of isolator and interacts with the strong shock integrated with the reflected shock of the reattachment shock, the second reflected shock of the second cowl shock when the back pressure ratio $PR = 7.0$. Due to the asymmetric separation vortex in the shock train zone, the core flow deflects to the cowl wall and the primary shock has already bifurcated, thereby forming the asymmetric "X" shape shock. In the meanwhile, the shock foot on the ramp wall is ahead of that on the cowl wall, which reveals the much thicker boundary layer on the ramp wall upstream shock train. As the back pressure ratio PR increased to 8.0, except for the similar flow structure of shock train to the back pressure ratio $PR = 7.0$, the shock train relocates upstream and the asymmetric structure of primary shock is improved. When the back pressure ratio PR is increased to 8.5, the primary shock relocates near the throat and forms Mach reflection. The secondary and tertiary shock of shock train changes its "X" shape shock into the oblique shock. At this time, the state of flow field is extremely unstable and unstart can be induced by a small variation of adverse pressure gradient which spreads along the near-wall subsonic region. Therefore, the critical maximum back pressure ratio PR of the flow without ejecting nozzle has been achieved at the back pressure ratio $PR = 8.5$.

Table 2
CFD result with air ejecting at $M = 2.41$.

m_{cap} (kg/s)	m_{eje} (kg/s)	M_{eje} (–)	m_{eje}/m_{cap} (%)	Imp_{bp} (%)
0.55	0.05	2.33	9.89	15.29

Fig. 12 shows the throttled flow structure with ejecting nozzle. At first, when the back pressure ratio $PR = 9.0$, the primary shock of shock train locates the entrance of the divergent section and forms the "λ" shape shock. Moreover, the second and tertiary shocks can be clearly seen and are similar to a normal shock. When the back pressure ratio PR is increased from 9.0 to 9.3, the primary shock turns into a curved shock in order to match the increasing back pressure, but the position of primary shock is almost not changed. At the point, the second and tertiary shocks cannot be clearly discerned. However, when the back pressure ratio PR is increased to 9.8, the primary shock further turns into a near-normal shock accompanied by slight relocation upstream and the second and tertiary shocks also completely disappear. As shown in Fig. 13, once the back pressure ratio PR is more than 9.8, the shock train suddenly jumps upstream, which induces the inlet unstart. Therefore, the critical maximum back pressure ratio PR of the flow with ejecting nozzle has been achieved at the back pressure ratio $PR = 9.8$. Furthermore, one can obtain another result that under the same back pressure ratio range, the upper and bottom compression foot relocates at the $x_r = 0.1179 \sim 0.1255$ m and $x_c = 0.1175 \sim 0.1224$ m, respectively, which means that the integrated shock decreases the near-wall ejecting flow so that the boundary layer on the ramp is thicker than one on the cowl. The CFD result with air ejecting at $M = 2.41$ is shown in Table 2. Through the air ejecting control, the resistance to back pressure quantitatively increased from the back pressure ratio $PR = 8.5$ to $PR = 9.8$, by approximately 15% along with the utilization of air ejecting mass about 9.89% mass flow rate of mainstream. Therefore, the ejecting control method is useful to increase the resistance to back pressure in inlet through turning regular reflection of primary shock into Mach reflection, a curved shock and even a near-normal shock.

4.3. Influence of cracking gas ejecting on shock/boundary layer interaction

The flow structure at the rear part of the isolator and fore part of the divergent section, and corresponding pressure distributions with air and cracking gas ejecting at $M = 2.41$ and $P_{t,eje} = 1.07 \times 10^6$ Pa are shown in Fig. 14 and Fig. 15, respectively. For air ejecting, the integrated shock impinges at $x_r = 0.1096$ m on the ramp side and subsequently forms a series of regular reflection between the cowl and ramp wall, but not enough to cause flow separation; for the cracking gas ejecting, the Mach reflection with large-scale Mach stem is formed at $x = 0.1075$ m, 0.1258 m and 0.1316 m, respectively. Especially at $x_r = 0.1075$ m, there are two Mach stems in the Mach reflection, namely, Mach stem of wall-attachment and local hanging Mach stem far from the ramp. Moreover, the wide range of aerodynamic subsonic bands behind the local hanging Mach stem and two other Mach stems of wall-attachment are generated and completely separated from the wall by ejecting flow. The two subsonic bands on the ramp side are connected by the supersonic region which is formed by expansion fan at the divergent section. At this point, the local shock train is also formed at $x_r = 0.1316 \sim 0.1462$ m and $x_c = 0.1258 \sim 0.1353$ m due to the large adverse pressure gradient induced by the Mach reflection.

Please cite this article in press as: Y. He et al., Investigation of boundary-layer ejecting for resistance to back pressure in an isolator, Aerosp. Sci. Technol. (2016), http://dx.doi.org/10.1016/j.ast.2016.04.016

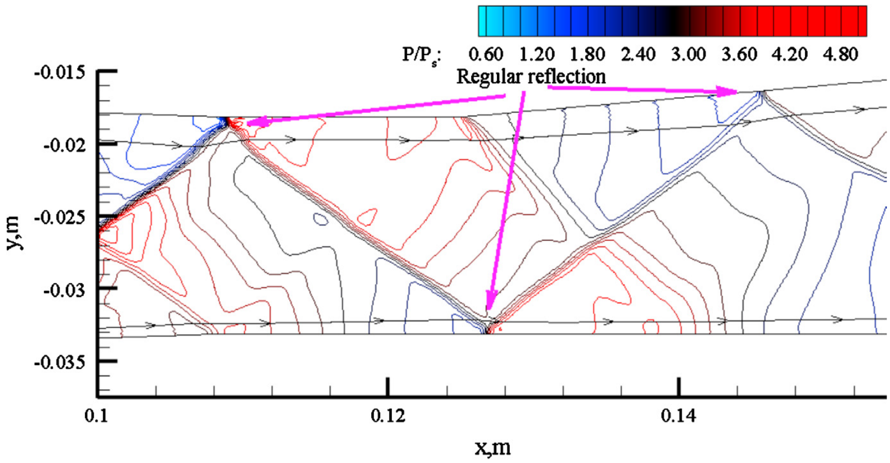

(a). Pressure contour of unthrottled flow with air ejecting

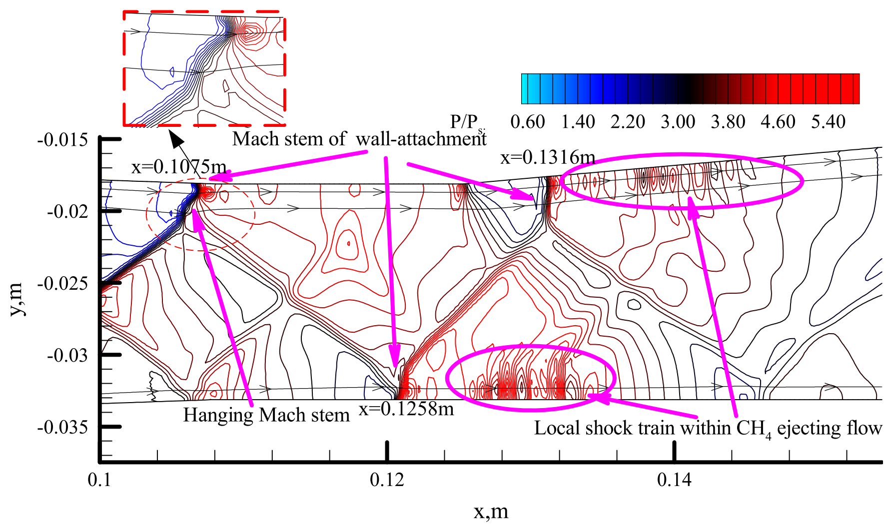

(b). Pressure contour of unthrottled flow with methane ejecting

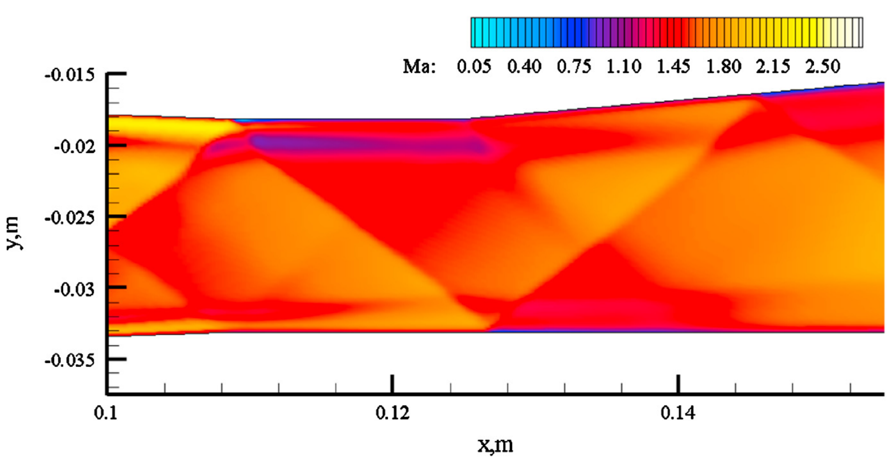

(c). Mach number of unthrottled flow with air ejecting

Fig. 14. Flow structure with air and cracking gas ejecting at the rear part of the isolator and fore part of the divergent section and $M = 2.41$, $P_{t,eje} = 1.07 \times 10^6$ Pa.

Table 3 quantitatively gives the CFD result with air and cracking gas ejecting at $M = 2.41$ and $P_{t,eje} = 1.07 \times 10^6$ Pa. According to a comparison result, the resistance to back pressure with cracking gas ejecting cannot be improved. The main reason for difference between the two is that although the momentum of ejecting cracking gas is greater than the ejecting air while the dynamic viscosity of ejecting cracking gas is less than the ejecting air, the local hanging Mach stem and Mach stems of wall-attachment on the ramp side greatly decrease the flow momentum behind the corresponding Mach stems, thereby causing the adverse pressure gradient to

Please cite this article in press as: Y. He et al., Investigation of boundary-layer ejecting for resistance to back pressure in an isolator, Aerosp. Sci. Technol. (2016), http://dx.doi.org/10.1016/j.ast.2016.04.016

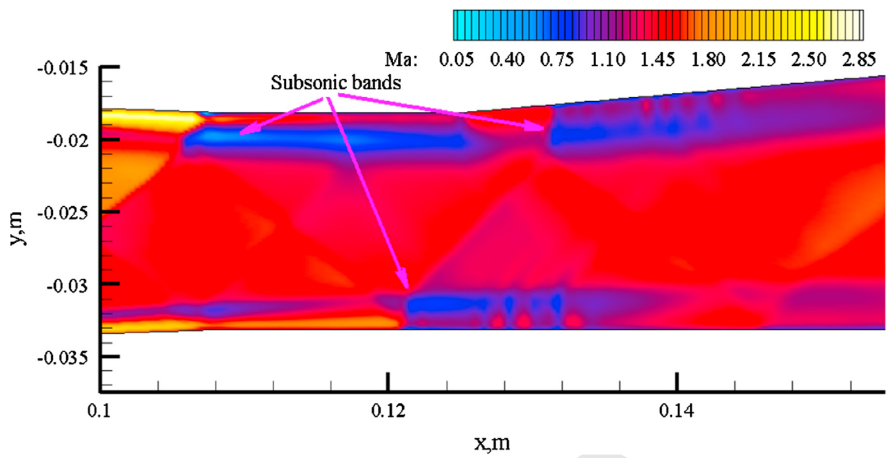

(d). Mach number of unthrottled flow with methane ejecting

Fig. 14. (*continued*)

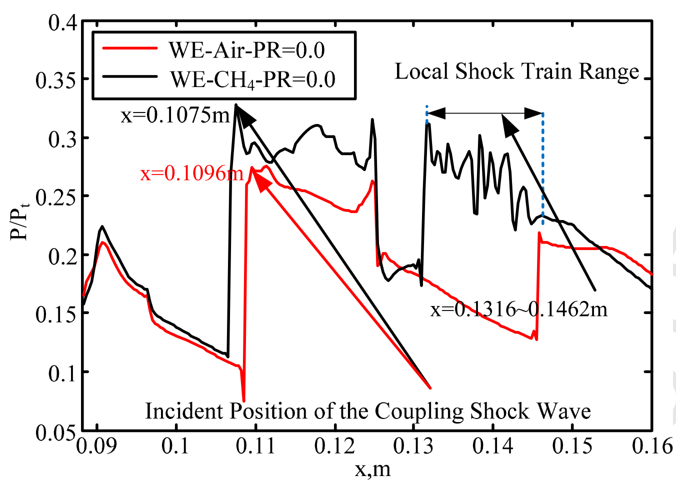

(a). Pressure distribution on the ramp surface

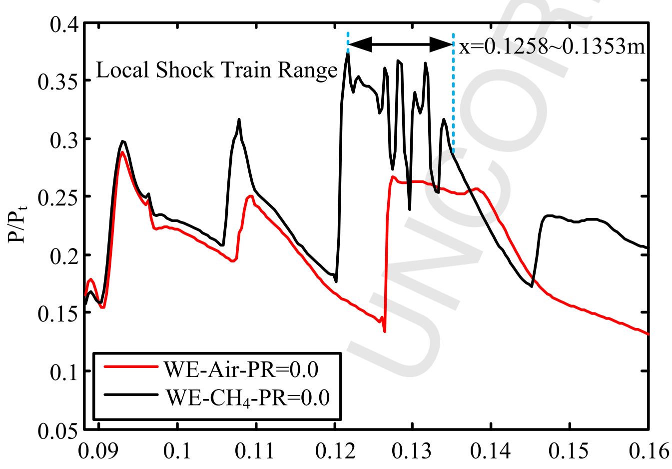

(b). Pressure distribution on the cowl surface

Fig. 15. Pressure distributions with air and cracking gas ejecting at $M = 2.41$ and $P_{t,eje} = 1.07 \times 10^6$ Pa.

easily propagate upstream mainly along the wide range of subsonic bands far from the ramp as the back pressure ratio *PR* increased. Therefore, it can be concluded that the formation of Mach stems can induce additional weakness, namely, the wide range of subsonic band, thereby significantly decreasing resistance to back pressure in the case of low ejecting total pressure.

4.4. Influence of ejecting total pressure of cracking gas on resistance to back pressure

Figures 16–17 show the flow structure and pressure distributions with cracking gas ejecting for different ejecting total pressures. When the ejecting total pressure is increased from $P_{t,eje} = 1.07 \times 10^6$ Pa to $P_{t,eje} = 4 \times 10^6$ Pa, all the Mach reflection in Fig. 14b is completely turned into the regular reflection and the corresponding reflection point gradually moves downstream. The main reason for the shock transformation is that the velocity of fluid ahead of local hanging Mach stem is significantly increased by the increasing ejecting total pressure so that Mach number of the fluid is greater than the minimum Mach number at given deflection angle of gas flow, thereby forming the regular reflection near wall. Moreover, it can be seen that both the reflected shock of integrated shock and the incident shock on the ramp side of the divergent section form a local hanging Mach stem far from the ramp. Meanwhile, the local shock train at $x_c = 0.1258 \sim 0.1353$ m in Fig. 14b also disappears completely while the range of local shock train at the divergent section is significantly narrowed at $P_{t,eje} = 3 \times 10^6$ Pa and then disappears at $P_{t,eje} = 4 \times 10^6$ Pa. In addition, the subsonic band behind the hanging Mach stem is gradually decreased as the ejecting total pressure increased.

Table 4 gives CFD result at different ejecting total pressures. It is not until the ejecting total pressure is increased to $P_{t,eje} = 3 \times 10^6$ Pa the resistance to back pressure is obviously increased. Moreover, the resistance to back pressure through using ejecting total pressure $P_{t,eje} = 3 \times 10^6$ Pa and $P_{t,eje} = 4 \times 10^6$ Pa quantitatively increases by 5.88% and 11.76%, respectively. The main reason is that the increase of ejecting total pressure indirectly enhances the ejecting momentum and decreases the dynamic viscosity of cracking gas. For the increase of ejecting momentum, when the original Mach reflection with Mach stem of wall-attachment and hanging Mach stem is turned into the regular reflection with the only hanging Mach stem as well as the ejecting momentum is sufficient to turn Mach reflection of divergent section into regular reflection with local shock train, the flow field of shock-wave system can be regard as the critical iconic feature which can increase resistance to back pressure. For the decrease of dynamic viscosity, it can prompt the random motion of molecules in the shear layer between ejecting cracking gas and core flow, thereby increasing the mixing of the momentum, mass and energy so that the

Please cite this article in press as: Y. He et al., Investigation of boundary-layer ejecting for resistance to back pressure in an isolator, Aerosp. Sci. Technol. (2016), http://dx.doi.org/10.1016/j.ast.2016.04.016

Table 3
CFD result with air and cracking gas ejecting at $M = 2.41$ and $P_{t,eje} = 1.07 \times 10^6$ Pa.

Ejecting material type	m_{cap} (kg/s)	m_{eje} (kg/s)	m_{eje}/m_{cap} (%)	Critical PR (–)	Imp_{bp} (%)	M_{eje} (–)	mv (kg m/s^2)	$\mu \times 10^5$ (kg/m s)
Air	0.55	0.05	9.79	9.80	15.29	2.33	47.10	2.87
CH_4	0.55	0.03	5.44	7.70	−9.41	2.29	58.52	2.37

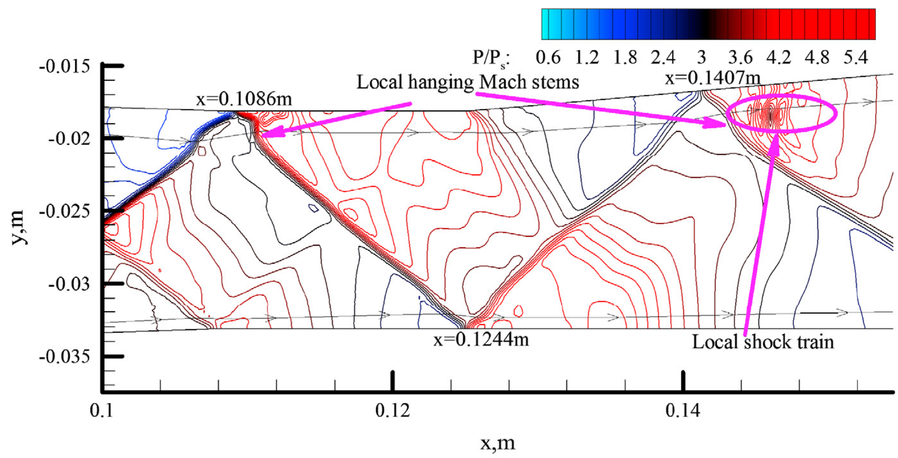

(a). Pressure contour of unthrottled flow with methane ejecting at $P_{t,eje}$ = 3 MPa, PR = 0.0

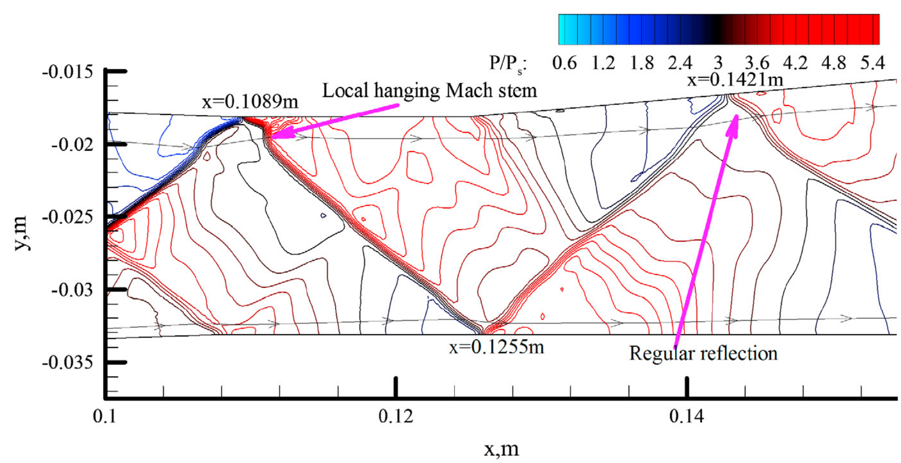

(b). Pressure contour of unthrottled flow with methane ejecting at $P_{t,eje}$ = 4 MPa, PR = 0.0

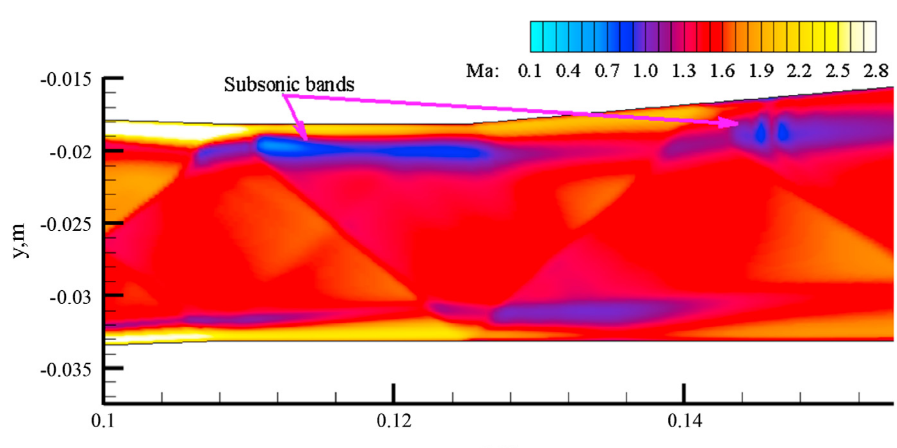

(c). Mach number contour of untrottled flow with methane ejecting at $P_{t,eje}$ = 3 MPa, PR = 0.0

Fig. 16. Flow structure for different ejecting total pressures at the rear part of the isolator and fore part of the divergent section, $M = 2.41$, $PR = 0.0$.

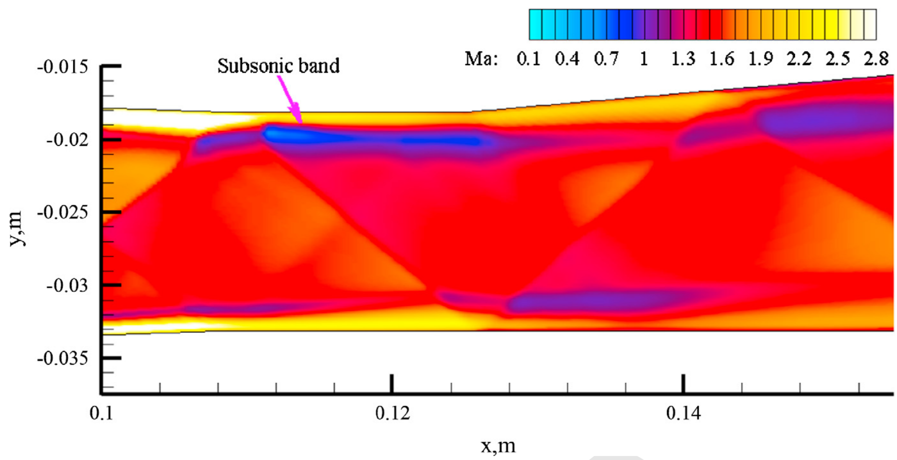

(d). Mach number contour of unthrottled flow with methane ejecting at $P_{t,eje}$ = 4 MPa, *PR* = 0.0

Fig. 16. (*continued*)

Table 4
CFD result at different ejecting total pressures and $M = 2.41$.

Case	$P_{t,eje}$ (Pa)	M_{eje} (–)	m_{eje} (kg/s)	mv (kg m/s^2)	$\mu \times 10^5$ (kg/m s)	Critical *PR* (–)	Imp_{bp} (%)
1	3×10^6	2.79	0.03	70.98	2.17	9.0	5.88
2	4×10^6	2.93	0.04	78.35	2.11	9.5	11.76

subsonic band is obviously narrowed. Therefore, the resistance to back pressure depends on the combined function of momentum and viscous dissipation.

Figures 18–19 give the throttled flow patterns and pressure distributions of shock/boundary layer interaction at $M = 2.41$, $P_{t,eje} = 4 \times 10^6$ Pa. As the back pressure ratio *PR* increased, the shock train always consists of a curved shock. When the curved shock relocates upstream, the curved shock becomes more symmetrical. Furthermore, it can be inferred from pressure distribution that when the back pressure ratio *PR* is increased to 9.0, local shock train is formed behind the bottom compression foot so as to induce the minor pressure fluctuation. However, when the back pressure ratio *PR* is increased from 9.0 to critical back pressure ratio *PR* 9.5, the local shock train gradually moves downstream and correspondingly pressure fluctuation is significantly enhanced, which indicates that the strength and range of the local shock train are increased. Therefore, the evolution of shock train with cracking gas ejecting is completely different from the throttled flow with air ejecting (see Fig. 12).

5. Conclusions

This paper investigates the control of shock/boundary-layer interaction and the resistance to back pressure with gas ejecting. CFD simulations in $M = 2.41$ inlet are performed to understand the complex flow phenomena, thereby revealing the physical mechanism and the control capability of the ejecting. The following are the main conclusions of this study:

1) According to the CFD quantitative results, the resistance to back pressure with air and cracking gas ejecting is increased by 15.29% and 11.76% along with the utilization of ejecting mass about 9.89% and 7.66% mass flow rate of mainstream at $P_{t,eje} = 1.07 \times 10^6$ Pa and $P_{t,eje} = 4 \times 10^6$ Pa, respectively. Therefore, through the reasonable set of position and ejecting condition of the Aft-Facing Step Nozzle (AFSN), the resistance to back pressure, whether the air ejecting or cracking gas ejecting, can be significantly increased.

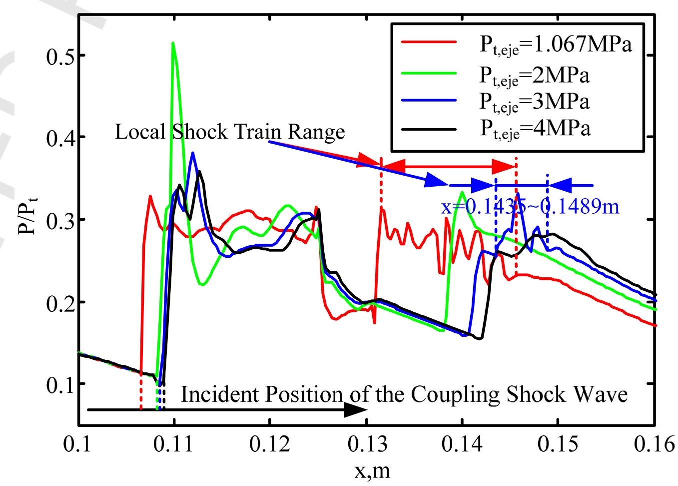

(a). Pressure distribution on the ramp surface for different ejecting total pressures

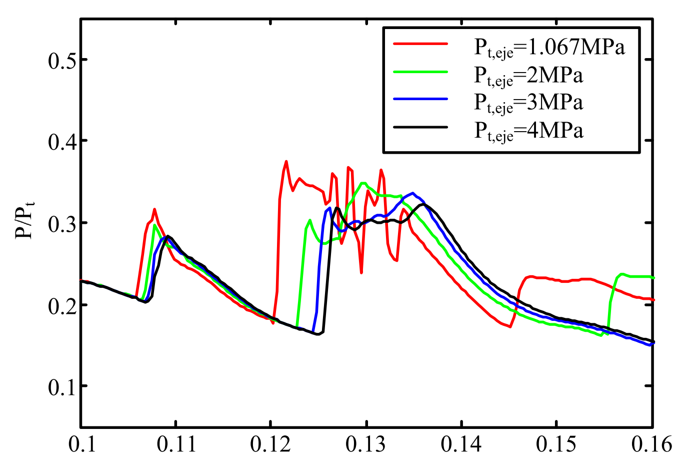

(b). Pressure distribution on the cowl surface for different ejecting total pressures

Fig. 17. Pressure distributions for different ejecting total pressures at $M = 2.41$, $PR = 0.0$.

Please cite this article in press as: Y. He et al., Investigation of boundary-layer ejecting for resistance to back pressure in an isolator, Aerosp. Sci. Technol. (2016), http://dx.doi.org/10.1016/j.ast.2016.04.016

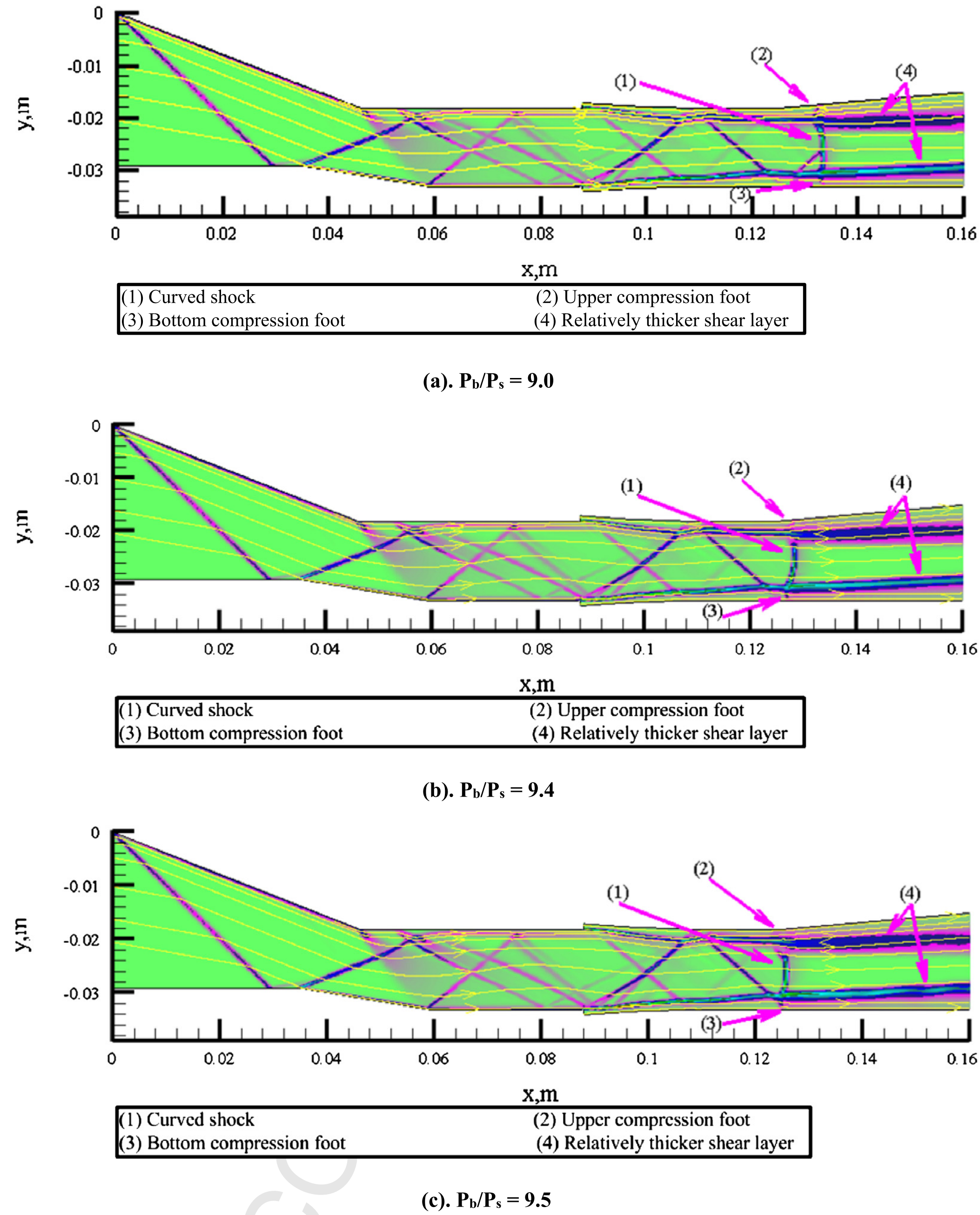

Fig. 18. Throttled flow patterns of shock/boundary layer interaction at the fore part of the duct, $M = 2.41$, $P_{t,eje} = 4 \times 10^6$ Pa.

2) The flow field characteristic with air and cracking gas ejecting is compared to reveal the difference of shock/boundary layer interaction and the propagating path of adverse pressure gradient. As the back pressure increased, the adverse pressure gradient can propagate upstream along the wide range of aerodynamic subsonic bands far from the wall, which are formed by the large-scale Mach stem of Mach reflection in the case of low ejecting total pressure. Furthermore, as the back pressure ratio gradually increased, for the air ejecting, the primary shock of shock train is turned regular reflection into Mach reflection, a curved shock and even a near-normal shock to match the downstream pressure rising compared to flow without ejecting, and the position of primary shock almost keeps unchanged while for the cracking gas ejecting, the primary shock always maintains a curved shock and slightly relocates upstream. However, when the back pressure ratio is increased above each critical back pressure ratio, the shock train suddenly relocates upstream, which induces the inlet unstart.

3) The influence of ejecting total pressure on flow field is further analyzed to understand the physical mechanism of the resistance to back pressure. The increase of the ejecting total pressure can indirectly increase the ejecting momentum and decrease the ejecting dynamic viscosity, which prompts the random motion of molecules in the shear layer between ejecting flow and core flow, thereby increasing the mixing of the momentum, mass and energy to narrow the subsonic band and suppress the adverse pressure gradient. Therefore, the resistance to back pressure depends on the combined function of momentum and viscous dissipation.

Conflict of interest statement

None declared.

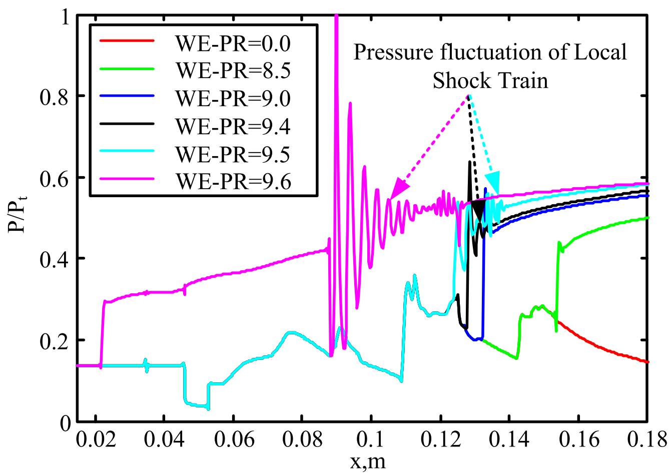

(a). Pressure distribution on the ramp surface for different back pressures

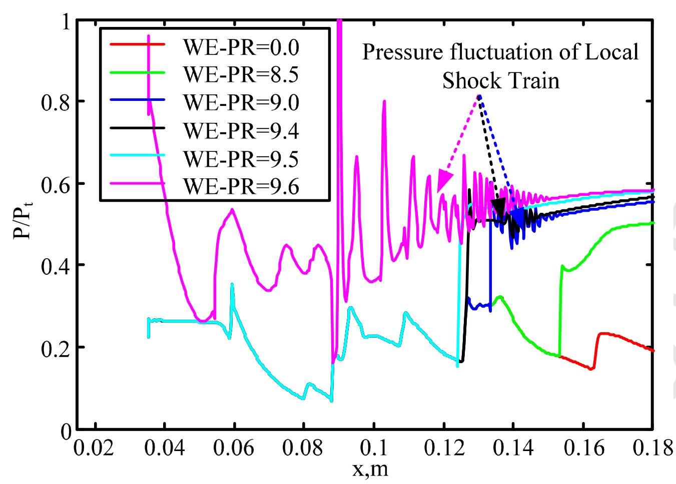

(b). Pressure distribution on the cowl surface for different back pressures

Fig. 19. Throttled pressure distributions of shock/boundary layer interaction at $M = 2.41$, $P_{t,eje} = 4 \times 10^6$ Pa.

Acknowledgement

This work was sponsored by the Foundation for Innovative Research Groups of the National Natural Science Foundation of China (No. 51121004).

References

[1] W. Heiser, D. Pratt, Hypersonic Airbreathing Propulsion, AIAA Education Series, AIAA, Washington, DC, 1994.
[2] E. Curran, W. Heiser, D. Pratt, Fluid phenomena in scramjet combustion system, Annu. Rev. Fluid Mech. 28 (1996) 323–360.
[3] K. Numbers, A. Hamed, Conservation coupling techniques for dynamic inlet-engine analysis, J. Propuls. Power 19 (3) (2003) 444–455.
[4] J.M. Delery, Shock wave/turbulent boundary layer interaction and its control, Prog. Aerosp. Sci. 22 (4) (1985) 209–280.
[5] A. Hamed, A. Kumar, Flow separation in shock wave boundary layer interactions, J. Eng. Gas Turbines Power 116 (1) (1994) 98–103.
[6] D. Schulte, A. Henckels, U. Wepler, Reduction of shock induced boundary layer separation in hypersonic inlets using bleed, Aerosp. Sci. Technol. 2 (4) (1998) 231–239.
[7] J. Haberle, A. Gülhan, Internal flowfield investigation of a hypersonic inlet at Mach 6 with bleed, J. Propuls. Power 23 (5) (2007) 1007–1017.
[8] J. Haberle, A. Gülhan, Investigation of the flow field of a 2D scram-jet inlet at Mach 7 with optional boundary layer bleed, AIAA 2007-5068, 2007.
[9] J. Syberg, J.L. Koncsek, Bleed system design technology for supersonic inlets, J. Aircr. 10 (7) (1973) 407–413.
[10] M.R. Saad, H. Zare-Behtash, A. Che-Idris, K. Kontis, Micro-ramps for hypersonic flow control, Micromachines 3 (2) (2012) 364–378.
[11] A.C. Idris, M.R. Saad, H. Zare-Behtash, K. Kontis, Luminescent measurement systems for the investigation of a scramjet inlet-isolator, Sensors 14 (4) (2014) 6606–6632.
[12] J.M. Oorebeek, H. Babinsky, Bleed and vortex generator effectiveness for separation prevention in a transonic diffuser, AIAA 2014-2793, 2014.
[13] R.R. Martis, A. Misra, Effect of microramps on separated swept shock wave–boundary-layer interactions, AIAA J. 52 (3) (2014) 591–603.
[14] J.C. Lin, Boundary layer control for aerofoils and wings, in: Boundary Layer and Flow Control, in: Its Principles and Application, vol. 2, Pergamon, Oxford, 1961, pp. 1170–1344.
[15] L.J. Souverein, J.F. Debieve, Effect of air jet vortex generators on a shock wave boundary layer interaction, Exp. Fluids 49 (5) (2010) 1053–1064.
[16] F.R. Menter, Two-equation eddy-viscosity turbulence models for engineering applications, AIAA J. 32 (8) (1994) 1598–1605.
[17] J.E. Bardina, P.G. Huang, T.J. Coakley, Turbulence modeling validation, AIAA 1997-2121, 1997.
[18] B.U. Reinartz, C.D. Herrmann, J. Ballmann, Aerodynamic performance analysis of a hypersonic inlet isolator using computation and experiment, J. Propuls. Power 19 (5) (2003) 868–875.
[19] R.H. Tindell, B.P. Willis, Experimental investigation of blowing for controlling oblique shock/boundary layer interactions, AIAA 1997-2642, 1997.